Tryptophan and Tyrosine Radicals in Ribonucleotide Reductase: A Comparative High-Field EPR Study at 94 GHz†

Günther Bleifuss,‡ Matthias Kolberg,‡ Stephan Pötsch,§ Wulf Hofbauer,‡ Robert Bittl,‡ Wolfgang Lubitz,‡,|| Astrid Gräslund,§ Günter Lassmann,‡,|| and Friedhelm Lendzian*,‡

Max-Volmer-Laboratorium für Biophysikalische Chemie, Institut für Chemie, Technische Universität Berlin, PC 14, Strasse des 17. Juni 135, D-10623 Berlin, Germany, and Department of Biophysics, Stockholm University, Arrhenius Laboratories, S-10691 Stockholm, Sweden

Received April 6, 2001; Revised Manuscript Received July 20, 2001

ABSTRACT: Tryptophan radicals, which are generated in the reconstitution reaction of mutants Y122F and Y177W of subunit R2 apoprotein of *E. coli* and mouse ribonucleotide reductase (RNR), respectively, with Fe^{2+} and oxygen, are investigated by high-field EPR at 94 GHz and compared with the tyrosine radicals occurring in the respective wild-type proteins. For the first time, accurate *g*-values are obtained for protein-associated neutral tryptophan free radicals, which show only a small anisotropy. The apparent hyperfine patterns observed in frozen solutions are very similar for tryptophan and tyrosine radicals in mouse subunit R2 at conventional X-band EPR. The radicals can, however, be discriminated by their different *g*-tensors using high-field EPR. Tryptophan radicals were postulated as reaction intermediates in the proposed radical transfer pathway of RNR. Furthermore, the data obtained here for the electronic structure of protein-associated tryptophan neutral free radicals are important for identification and understanding of the functional important tryptophan radicals which occur in other enzymes, e.g., DNA photolyase and cytochrome *c* peroxidase, where they are magnetically coupled to other radicals or to a metal center.

Ribonucleotide reductase (RNR)[1] catalyzes the reduction of ribonucleotides to deoxyribonucleotides and is therefore a key enzyme for DNA synthesis. Class I ribonucleotide reductases consist of two proteins, R1 and R2, both of which are homodimers. R1 contains the binding sites for substrate and the allosteric effectors, and R2 carries a dinuclear iron site and, in the active state, a tyrosine radical. The three-dimensional structures of R1 (*1*) and R2 (*2*) from *Escherichia* (*E.*) *coli* and of R2 from mouse (*3*) have been determined by X-ray diffraction. In the active enzyme, the diiron center in R2 is in the diferric $Fe^{III}Fe^{III}$ state and couples antiferromagnetically to an $S = 0$ ground state. The tyrosine radical, Y122*, is in close vicinity (*4*) to the diiron center. The catalytic reaction in R1 is believed to start from a transient thiyl radical close to the substrate, at cysteine C439, which is generated by coupled electron/proton transfer from C439 to the tyrosine radical Y122* in subunit R2 (*4*−*9*). The postulated radical transfer pathway involves also a tryptophan radical intermediate (W48 in *E. coli*).

Removal of the dinuclear iron center from R2 is accompanied by a loss of the radical state at Y122 leading to the inactive apoprotein R2. The catalytically essential iron/radical center can be reconstituted in a reaction of the iron-free apoprotein with ferrous iron and molecular oxygen (*10*, *11*). Thereby an intermediate high-valent $Fe^{III}Fe^{IV}$ state (X) is formed in this reaction, which is capable of oxidizing the nearby Y122 to its radical form (*12*−*14*).

Several mutants have been constructed where Y122 is replaced by other amino acids. Their iron reconstitution and concomitant oxygen activation reactions have been investigated with the aim to generate other amino acid radicals than tyrosine and study their possible functional activity (*11*−*17*). Thereby neutral tryptophan radicals have been identified in two mutants, R2-Y122F (*16*, *17*) and R2-Y177W (*15*), and characterized by conventional EPR and ENDOR spectroscopy combined with selective isotope labeling (*11*, *15*−*17*).

Protein-linked tryptophan cation radicals, associated with a heme iron, have already been detected earlier by EPR and ENDOR spectroscopy in cytochrome *c* peroxidase (*18*). In this system, the intrinsic hyperfine structure and *g*-values of the tryptophan radical were, however, obscured by the interaction between the electron spins on the heme iron and

† Research supported by the Deutsche Forschungsgemeinschaft (Grants DFG La 751/2-2 and Le 812/2-1 to G.L. and F.L. and Grant Lu 315/15-1 to W.L. and F.L.).

* Corresponding author. Fax: (++49) 30 314 21122; E-mail: lendzian@echo.chem.tu-berlin.de.

‡ Max-Volmer-Laboratorium für Biophysikalische Chemie und Biochemie.

§ Department of Biochemistry and Biophysics, Stockholm University.

|| Present address: Max-Planck-Institut für Strahlenchemie, Stiftstrasse 34-36, D-45470 Mülheim/Ruhr, Germany.

[1] Abbreviations: RNR, ribonucleotide reductase; EPR, electron paramagnetic resonance; ENDOR, electron nuclear double resonance; hf, hyperfine; Y122*, functional tyrosine radical in wild-type RNR subunit R2 from *E. coli*; Y177*, functional tyrosine radical in wild-type RNR subunit R2 of mouse; W111*, transient tryptophan radical during reconstitution of mutant apoprotein R2-Y122F of *E. coli* with Fe^{2+}; W177*, transient tryptophan radical during reconstitution of mutant apoprotein R2-Y177W of mouse with Fe^{2+}.

10.1021/bi010707d CCC: $20.00
Published on Web 11/17/2001

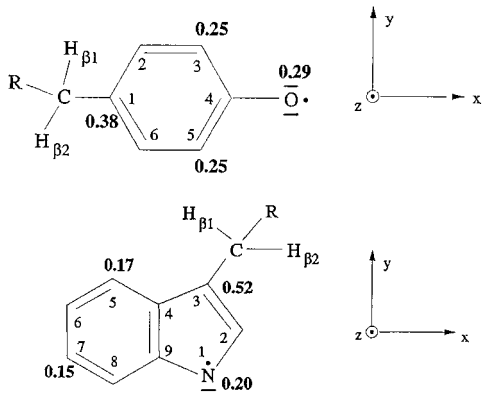

FIGURE 1: Molecular structures, numbering schemes, and *g*-tensor axis orientations for tyrosine (top) and tryptophan radicals. The boldface numbers give the π-spin densities at the respective positions derived from EPR and ENDOR experiments for tryptophan radicals (*17*), and for tyrosine radicals (*40*, *41*).

on the tryptophan radical. The diiron center in R2 of RNR is at a distance of ~4 and ~5 Å from the tryptophan radicals W111* and W177* in R2-Y122F and R2-Y177W, respectively. More important, the diiron center is in the diferric state and couples antiferromagnetically to an $S = 0$ ground state (*19*). Therefore, the tryptophan neutral radicals W111* and W177* generated in the R2 mutants have, at low temperatures ($T < 100$ K), spectroscopic characteristics of isolated free radicals.

Here, we report first high-field EPR studies on these protein-linked neutral tryptophan free radicals (Figure 1). Full hyperfine (*hf*)-tensors and for the first time accurate values for the *g*-tensor were obtained from spectra simulations and fits for two tryptophan neutral radicals and compared with those of the tyrosine radicals (Figure 1) in the respective wild-type R2. It is shown that the *g*-tensor is a fingerprint for the particular type of radical, which may be used to identify these different radicals even in cases where different protein environments induce changes of the *hf* structure.

MATERIALS AND METHODS

Sample Preparation. Overproduction of R2 was achieved in *E. coli* strain MC1009 pGP1-2 pTB2 for wild-type *E. coli*, in strain MC1009 pGP1-2 pMK5 for mutant Y122F (radical W111*) of *E. coli*, and in strains BL21(DE3) pLysS pETR2 and BL21(DE3) pLysS pETR2-Y177W for wild-type and mutant Y177W of mouse as described in (*15*, *17*). Wild-type and mutant R2 were isolated and purified as in (*15*, *17*, *20*). Freshly prepared and concentrated wild-type R2 (0.5 mM) of *E. coli* exhibited a radical yield for Y122* of about 1.0 per R2. Y177* in native R2 of mouse was generated by reconstitution of the apoprotein with ferrous iron and oxygen as described in (*20*). Tryptophan radicals were generated from mutant proteins Y122F and Y177W by reconstitution of the apoprotein (*11*, *15*, *16*); they have lifetimes of several minutes at room temperature. Apoprotein R2 was concentrated typically to 1 mM before reconstitution. After mixing of the aerobic apoprotein with anaerobic ferrous sulfate solutions, EPR samples were quickly filled (40−60 s) into quartz capillaries for W-band EPR (0.5 mm i.d., 0.9 mm o.d.) and frozen immediately in liquid nitrogen.

EPR Spectroscopy. Continuous-wave high-field EPR experiments at 94 GHz (W-band) were performed on a Bruker Elexsys 680 spectrometer. Spectra were recorded at 80 K. Low microwave power, typically only a few microwatts, was used in order to avoid saturation effects. For precise *g*-tensor values, the microwave frequency was measured by a frequency counter, which is integrated in the spectrometer. The magnetic field was calibrated with a *g*-standard [Li:LiF, $g = 2.002293(2)$, (*21*)] at two different frequencies (typically 94 and 94.3 GHz). All spectra were recorded in the "persistent mode" of the superconducting magnet, using the room-temperature coils for the field sweep. Thereby a high linearity and stability of the field was ensured. The design of the W-band EPR resonator (H_{102}-cavity) ensures high sensitivity and a small active sample dimension (approximately 0.5 mm diameter and 1.5 mm heighth). This leads to a high-field homogeneity over the active sample volume (better than 0.05 mT) which allows excellent simultaneous resolution of *g*- and *hf*-tensor components.

Simulation of Spectra. The EPR powder spectra have been analyzed using a program for simulation and fitting of EPR spectra with anisotropic *g*- and *hf*-tensors described in (*17*). The spectra were simulated by computing the resonant field position correct to second order at the given microwave frequency dependent on the orientation of the tensors with respect to the external magnetic field (*22*). The superposition of all orientations for the randomly oriented powder-like sample was performed employing a spiral approach (*23*), typically using 1000 grid points. No restrictions for the relative orientation of the principal axes of the different tensors exist. The principal axis system of the *g*-tensor serves as a reference system, and the orientations of the *hf*-tensors, $\mathbf{A}_i$, are given by three Euler angles. The resulting histogram of resonant field positions is folded with a combined Lorentzian and Gaussian line shape function, finally yielding the derivative EPR spectrum. A nonlinear least-squares routine is used to find the optimum set of parameters for best simulating a given experimental spectrum.

DFT Calculations. Density functional theory (DFT) calculations were performed to obtain principle values and axes of the *g*-tensor of the tryptophan neutral radical. The ADF package (*24*) was used for the geometry optimization and the *g*-tensor calculation. As a model for the tryptophan radical, 3-CH_3 indole was used. The geometry optimization was performed at the scalar relativistic ZORA level with the Becke (*25*) and Perdew (*26*) gradient correction and correlation terms, respectively. For the *g*-tensor calculation, the spin−orbit relativistic ZORA level was used.

RESULTS

W111, g- and hf-Tensors.* Figure 2 shows the obtained W-band EPR spectra for the tryptophan radical W111* in mutant R2-Y122F compared with the tyrosine radical Y122* in wild-type R2 of *E. coli*. The spectra exhibit good *g*-resolution (in particular for the tyrosine radical), as expected for the higher microwave frequency, 94 GHz compared with 9.4 GHz at conventional X-band EPR, and at the same time also good hyperfine resolution. This indicates that the radicals have a well-defined environment and structural heterogeneities of the protein, which would give rise to *g* or hyperfine strain, are not prominent.

The EPR spectrum of W111* exhibits an almost symmetrical four-line pattern with resolved subsplittings, in

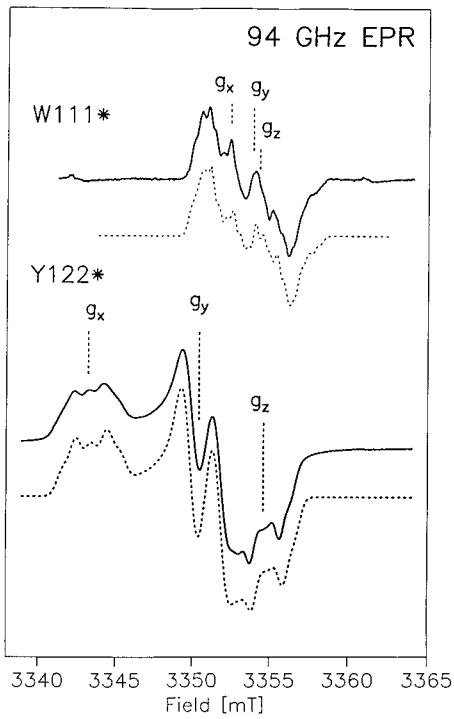

FIGURE 2: Comparison of high-field EPR spectra (94 GHz) of tryptophan radical W111* in *Escherichia coli* mutant R2-Y122F and tyrosine radical Y122* in *Escherichia coli* wild-type R2. Experimental conditions: Y122*: $T = 20$ K, microwave power (mw) = 2 μW, modulation amplitude (ma) = 0.4 mT, modulation frequency (mf) = 100 kHz; W111*: $T = 40$ K, mw = 2 μW, ma = 0.1 mT, mf = 100 kHz; accumulation times: 6 min and 2 min for W111* and Y122*, respectively. The dashed traces are best simulations using the *g*- and *hf*-values given in Tables 1−3 and single-component Gaussian line widths of 0.18 and 0.2 mT for W111* and Y122*, respectively.

particular on the low-field side. This already indicates that the spectrum is dominated by hyperfine interaction and *g*-anisotropy is small. Simulations and fits of the EPR spectrum were performed using one anisotropic ^{14}N *hf*-tensor, the almost isotropic *hf*-tensor data of two β-protons from the tryptophan side chain, and the anisotropic *hf*-tensors of two ring protons from ENDOR (*17*) as starting values. The four-line structure in the EPR spectrum of W111* is due to the two β-proton hyperfine couplings, one of them being approximately twice as large as the other (Table 3). The subsplittings which are particularly seen on the low-field side result from the two anisotropic α-protons. The outermost shoulders, best seen on the high-field side, are due to the largest ^{14}N-*hf*-tensor component ($\mathbf{A}_z$). The final fit of the spectrum (dotted line) yielded all three *g*-tensor components for W111* (Table 1), the *hf*-tensor components of ^{14}N and four protons and the relative *g*- and *hf*-tensor axis orientations are collected in Table 3. The *g*-values of W111* given in Table 1 represent the first accurate *g*-tensor data for a neutral tryptophan free radical and show only small anisotropy as compard to oxygen-containing radicals such as tyrosine or quinones (*27*).

Important information about the electronic structure of the tryptophan radical W111* is the orientation of its *g*-tensor axes with respect to its molecular structure. The fit of the high-field EPR spectra of W111* (Figure 2) yields only relative orientations between *g*- and *hf*-tensor axes. However, the orientations of the *hf*-tensor axes are clearly related to the molecular structure. The fit for W111* (Figure 2 and Table 3) shows that the axis of the largest ^{14}N-*hf*-tensor component is parallel to that of the lowest *g*-value, g_z. The axial symmetry ($\mathbf{A}_x = \mathbf{A}_y$) and the large anisotropy of the *hf*-tensor indicate significant π-spin density ($\rho^\pi \approx 0.2$; see ref *17*) at the ^{14}N nucleus of the tryptophan radical W111*. For this case, the largest ^{14}N-*hf*-tensor component is expected for the out-of-plane axis *z* (see Figure 1). The finding, that the g_z-axis is perpendicular to the molecular plane, is found for most π-radicals with planar π-systems, and is also expected from theory (*28*).

Table 1: *g*-Tensor Principal Values for Tryptophan and Tyrosine Radicals[a]

	g_x	g_y	g_z
W111*[a]	2.0033(1)	2.0024(1)	2.0021(1)
W177*[a]	2.0035(1)	2.0025(1)	2.0023(1)
W*[b]	2.00406	2.00284	2.00218
Y122*[a,c]	2.0091(1)	2.0046(1)	2.0021(1)
Y177*[a,c]	2.0076(1)	2.0044(1)	2.0021(1)

[a] This work, from simulated EPR spectra (Figures 2 and 3); numbers in parentheses are errors in the last digit. [b] Calculated values for the 3-CH_3-indole neutral radical. For orientation of *g*-axes, see text. [c] Values agree within experimental error with those given in (*20*, *34*). For Y177*, a hydrogen bond was verified by ENDOR (*20*), which is absent in Y122* (see text).

The orientation of the in-plane *g*-tensor axes g_x and g_y can be obtained from the *hf*-tensor axes of the α-protons directly attached to the π-system, which are known to exhibit large anisotropy within the molecular plane. For an isolated C−H fragment, where C is a carbon of the π-system, the axis of the largest tensor component is expected to be in the molecular plane perpendicular to the C−H bond (*29*). The simulations of the high-field EPR spectrum of W111* indicate that the axis of g_x forms an angle of about 10° with the axis of the largest *hf*-tensor component of one α-proton. For a second α-proton, 60° is obained for the corresponding angle. Earlier density functional calculations of the tryptophan neutral radical indicated significant carbon π-spin densities and corresponding large α-proton *hf*-couplings only for positions 5 and 7 (ref *17*; see Figure 1). Due to the similar magnitudes of their respective *hf*-tensor components, it is not possible to assign either of these observed *hf*-tensors to position 5 or 7, thus leaving two possible orientations for the g_x-axis in the molecular plane: either 10° or 60° with respect to the largest *hf*-tensor axis of position 5, which is expected to be parallel to the molecular *x*-axis (Figure 1). Based on theoretical considerations (see below), we prefer the assignment where the g_x-axis forms an angle of only 10° with the molecular *x*-axis.

DFT Calculations. Since the simulations of the EPR spectra allowed two possible orientations of the g_x-axis in the molecular plane (see above), we performed DFT calculations to obtain a theoretical value for the *g*-tensor principle values and axes. The calculated principle values are given in Table 1 together with the experimental results. The principal axis corresponding to the smallest *g*-tensor component g_z is perpendicular to the molecular plane. The principal axis corresponding to the largest *g*-tensor component g_x forms an angle of 20° with the molecular *x*-axis (Figure 1), in favor of the assignment with the smaller of the two angles, consistent with the EPR simulations.

Table 2: Hyperfine Tensor Principal Values (mT) for Tyrosine Radicals[a]

	Y122*			Y177*		
position[b]	$\mathbf{A}_x$[c]	$\mathbf{A}_y$[c]	$\mathbf{A}_z$[c]	$\mathbf{A}_x$[c]	$\mathbf{A}_y$[c]	$\mathbf{A}_z$[c]
Hβ_1	2.17	1.96	2.06	2.15	1.90	2.14
Hβ_2	<0.2	<0.2	<0.2	0.95	0.25	0.57
H3	0.96	0.28	0.70	0.91	0.44	0.66
H5	0.96	0.28	0.70	0.75	0.49	0.58

[a] This work, values from simulations of the spectra (Figures 2 and 3). [b] See molecular structures (Figure 1). [c] *z*-axis is collinear with molecular axis (Figure 1); x- and y-axes deviate from the respective molecular axes by approximately ±12°, for H3 and H5; signs not determined; from theory, values for H3 and H5 should be negative; estimates error: ±0.05 mT. Hyperfine tensor values of Y122* are in agreement with those obtained by ENDOR in (*42*).

*Comparison with Y122**. In contrast to the case of tryptophan radical W111*, the EPR spectrum of the tyrosine radical Y122* in wild-type R2 of *E. coli* (Figure 2, lower trace) is very asymmetric, which indiates a dominating large *g*-anisotropy. A fit to the EPR spectrum (dotted line) yielded the *g*- and *hf*-tensor data collected in Tables 1 and 2. The *g*-anisotropy is fully resolved at 94 GHz, allowing an immediate discrimination between these two types of radicals. The hyperfine structure in the spectrum arises from one large almost isotropic β-proton coupling, which gives rise to the splitting of the g_y-component, and two anisotropic α-proton *hf*-tensors, which have large components only for the g_x and g_z directions. The g_x-axis is assumed to be parallel to the C═O bond (*30*, *31*; see Figure 1). The α-proton *hf*-tensors are assigned to the protons at positions 3 and 5 based on earlier quantum chemical calculations (*32*). The axes of their largest *hf*-tensor components ($\mathbf{A}_x$) form angles of +12° and −12° with the g_x-axis.

W177 and Y177**. The advantage of high-field EPR for discrimination of tryptophan and tyrosine radicals is clearly demonstrated in Figure 3, where the X-band and W-band EPR spectra of the tryptophan radical W177* of mutant Y177W and the tyrosine radical Y177* of wild-type mouse R2 are compared. At X-band (9.4 GHz), both radicals yield surprisingly similar spectra (Figure 3A,B), which are dominated in both cases by the large and almost isotropic hyperfine splitting of one β-proton of the side chain. However, at W-band (94 GHz), the spectra of both radicals are very different. The spectrum of Y177* is now much broader and dominated by a large *g*-anisotropy (Figure 3D), whereas that of W177* shows much less change (Figure 3C). Simulations and fits of the high-field EPR spectrum of W177* (dotted trace, Figure 4) using the *hf*-tensor of one β-proton from the side chain and two anisotropic *hf*-tensors from two ring protons from ENDOR (*15*) as starting values yielded all three *g*-tensor components given in Table 1. The final proton and nitrogen *hf*-tensor values including the relative orientations of *g*- and *hf*-tensor axes obtained from the fits of the high-field EPR spectra of W177* are collected together with those for W111* in Table 3. Note the large difference of the *hf*-tensor values from protons Hβ_1 and Hβ_2 of W177* as compared with W111*, which is disussed below. The *g*-tensor and *hf*-tensor values obtained from fits to the high-field EPR spectrum of the tyrosine radical Y177* are given in Tables 1 and 2.

All three *g*-tensor components of the tryptophan radicals W111* in R2-Y122F of *E. coli* and W177* in R2-Y177W of mouse agree within experimental error. The *g*-tensor values obtained from fits of the high-field EPR spectra of the tyrosine radicals Y122* and Y177* are quite different from those of the tryptophan radicals. The g_z values are very similar for both types of radicals since they are π-radicals, but the g_y and g_x values are very different and may serve as molecular fingerprints of the particular type of radical. There is an interesting difference between the g_x-values of the two tyrosine radicals Y122* and Y177*, see below.

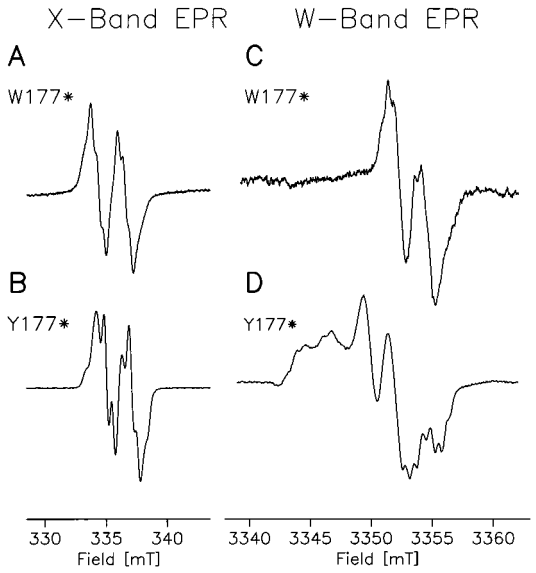

FIGURE 3: Comparison of X-band (A,B) and W-band (94 GHz, C,D) EPR spectra of the tryptophan radical W177* in mouse mutant R2-Y177W and the tyrosine radical Y177* in mouse wild-type R2. Experimental conditions: (A,B): T = 20 K, mw = 10 μW, ma = 0.1 mT, mf = 12.5 kHz; (C): T = 20 K, mw = 2 μW, ma = 0.1 mT, mf = 100 kHz; (D): T = 20 K, mw = 2 μW, ma = 0.4 mT, mf = 100 kHz.

DISCUSSION

g-Values of Tryptophan versus Tyrosine Radicals. The observed much smaller *g*-anisotropy of tryptophan radicals W111* and W177* (Table 1) as compared with the tyrosine radicals Y122* and Y177* can be understood qualitatively in the frame of the *g*-factor theory of Stone (*28*). According to (*28*), the out-of-plane component, g_z, of the *g*-tensor of a planar π-radical should be equal to the free electron value (g_e = 2.002319), which is indeed observed for both tryptophan and tyrosine radicals, whereas the in-plane components are shifted by $\Delta g_{x,y} = g_{x,y} - g_e$ toward higher values. This shift originates predominantly from excitations of an electron from a nonbonding lone pair orbital (at the oxygens in the case of tyrosine, or at the nitrogen in the case of tryptophan) into the half-filled π-orbital (*28*). For the *x*-component, it is given by

$$\Delta g_x = 2\xi\rho^{\pi}c_y^2/\Delta E_{n\pi^*} \quad (1)$$

where ξ is the spin−orbit coupling constant, ρ^{π} the π-spin density, and c_y the orbital coefficient of the p_y contribution to the lone pair orbital of the respective nucleus (*27*, *28*, *30*). $\Delta E_{n\pi^*}$ is the energy difference between the lone pair and half-filled π^* orbitals. An analogous expression is obtained for Δg_y. The small deviations of g_x and g_y from the free electron value (2.002319) observed for W111* and

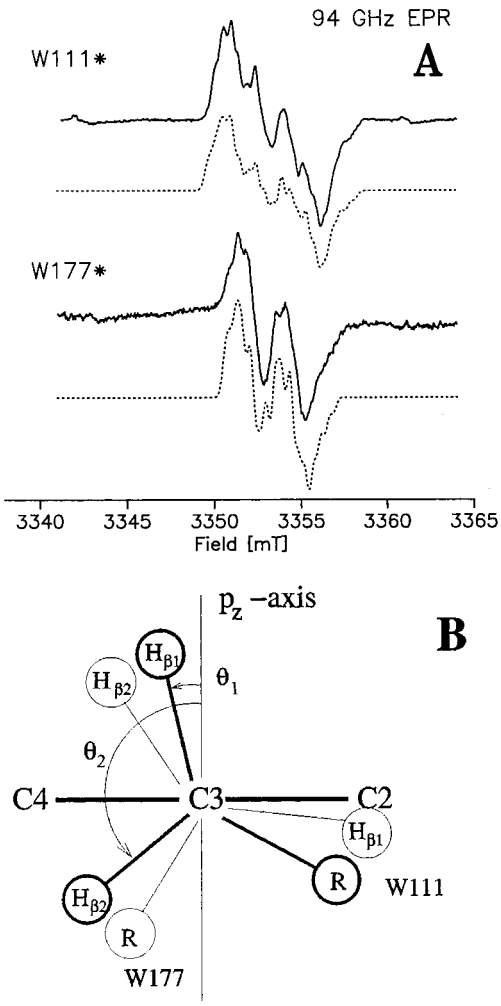

FIGURE 4: Comparison of different tryptophan radicals. (A) High-field EPR spectra (94 GHz) of W111* in *Escherichia coli* mutant R2-Y122F and W177* in mouse mutant R2-Y177W. The dashed traces are best simulations using the *g*- and *hf*-tensor values given in Tables 1 and 3 and a single-component Gaussian line width of 0.18 and 0.2 mT for W111* and W177*, respectively. (B) Edge-on view of tryptophan (compare Figure 1) showing the side chain orientations for radical W111* (boldface) and W177* (normal). The dihedral angles $\theta_1 = 13°$ and $\theta_2 = 133°$ shown for the β-protons of W111* are calculated from their isotropic *hf*-couplings (see text).

Table 3: Hyperfine Tensor Principal Values (mT) for Tryptophan Radicals[a]

	W111*			W177*		
position[b]	$\mathbf{A}_x$[c]	$\mathbf{A}_y$[c]	$\mathbf{A}_z$[c]	$\mathbf{A}_x$[c]	$\mathbf{A}_y$[c]	$\mathbf{A}_z$[c]
Hβ_1	2.70	2.75	2.83	<0.2	<0.2	<0.2
Hβ_2	1.38	1.38	1.38	2.25	2.25	2.25
^{14}N1	<0.1	<0.1	1.05	<0.1	<0.1	0.94
H5	0.68	<0.1	0.50	0.56	<0.1	0.46
H7	<0.1	0.61	0.51	0.16	0.63	0.52

[a] This work, values from simulations of the spectra (Figures 2 and 3). [b] See molecular structure (Figure 1); for protons Hβ_1 and Hβ_2, see Figure 4. [c] *z*-axis is collinear with molecular *z*-axis (Figure 1); *x*-axis for H5 deviates ≈10°, and *y*-axis for H7 deviates ≈60° from the g_x-axis (see text); signs not determined; from theory, values for H5 and H7 should be negative; estimated error: ±0.05 mT. Hyperfine tensor values are in agreement with those obtained by ENDOR in (*15*, *17*).

W177* as compared with those of Y122* and Y177* are due to the fact that spin density in the tryptophan neutral radicals is mainly localized on carbon 3 ($\rho^\pi \approx 0.5$) and, to a lesser extent, on nitrogen 1 ($\rho^\pi \approx 0.2$) [see Figure 1 (*15*, *17*)]. Both these nuclei have considerably lower spin−orbit coupling constants as compared with oxygen ($\xi = 28$, 76, and 151 cm^{-1} for C, N, and O, respectively; ref *29*). For the tyrosine radicals, however, the shifts of g_x and g_y are much larger due to their large spin density on the oxygen atom ($\rho^\pi \approx 0.3$, see ref *20*). It is interesting to note that the ratio of the Δg_x-values of the tryptophan radicals W111* and W177* (0.0011) versus the Δg_x-values of the tyrosine radicals Y177* and Y122* (0.0053 and 0.0066, Table 1) is reproduced by eq 1 almost quantitatively when using the respective values for ξ and only one lone pair orbital for the nitrogen in the tryptophan radicals, but two lone pair orbitals for the oxygen in the tyrosine radicals. The *g*-anisotropy for the tryptophan radical calculated by DFT is larger than observed experimentally. However, the relatively small shift of g_y compared to g_x is reproduced well in the calculations. We observed a similar overestimation of the *g* anisotropy in calculations, e.g., for quinone radicals.

There is an interesting difference of the g_x-value of Y122* and Y177*, which was already earlier interpreted as a result of a hydrogen bond to the oxygen in Y177* (*20*), which is absent in Y122* (*20*, *34*). Hydrogen bonds, and in general electrostatic interactions, have been shown to reduce the g_x-value for tyrosine radicals (*20*, *30*) and for quinone anion radicals (*27*, *35*). It can be qualitatively explained by a stabilization of the lone pair orbital, which increases $\Delta E_{n\pi^*}$ in eq 1, thereby reducing Δg_x.

g-Tensor Axes in W111.* Important information besides the magnitude of the *g*-tensor principal values is the orientation of the respective *g*-tensor axes. This is required in order to understand, e.g., the flavin/tryptophan radical pair signals observed in DNA photolyase (*33*) or, e.g., to deduce the radical orientations from single-crystal studies. The DFT calculations show that the g_z-axis is perpendicular to the molecular plane and the g_x-axis forms an angle of 20° with the molecular *x*-axis. This finding can be rationalized within the frame of the *g*-tensor theory by Stone (*28*). According to eq 1, the shift of the g_x component, Δg_x, is proportional to the orbital coefficient c_y of the contribution of the p_y orbital to the lone pair orbital. Since in the tryptophan radical only the nitrogen exhibits one lone pair orbital, which is oriented approximately along the molecular *y*-axis, the g_x-axis is expected to be perpendicular to *y* in the molecular plane, i.e., approximately parallel to the molecular *x*-axis (Figure 1). The calculated angle of 20° between the g_x-axis and the molecular *x*-axis from DFT corresponds well with this reasoning and one orientation obtained from the EPR simulations for W111* with an angle of 10° between these two axes (see Table 3).

Radical Identification via g- and hf-Tensors. A more general aspect of this work concerns the identification of protein-associated radicals, which is difficult when using standard X-band EPR methods alone. Radicals in proteins are mostly immobilized and exhibit solid-state powder EPR spectra, even in liquid solutions, due to the slow rotational motion of the large protein (*36*). This leads to only partially resolved hyperfine patterns, which considerably hampers a unique identification. This is demonstrated for W111* and W177* in Figure 3. The spectra of the tyrosine radical Y177* and the tryptophan radical W177* look surprisingly similar at X-band. In such cases, additional methods such as isotopic

labeling, as done previously for W111* and W177* (*11*, *15*, *16*), or site-directed mutagenesis are required for a unique identification. However, at higher EPR frequencies (W-band, 94 GHz), the spectrum of Y177* reveals the typical *g*-anisotropy of a tyrosine radical, which allows a clear distinction between these types of radicals without further isotope labeling.

On the other hand, as can be seen in Figure 4A, the hyperfine structures of the high-field EPR spectra of the same type of tryptophan neutral radicals, W111* and W177*, can look very different. This clearly shows that the observed hyperfine structure is less suited for radical identification. At first glance, this seems surprising and gives the impression that these spectra originate from different types of radicals. Closer inspection of both tryptophan neutral radicals by ENDOR (*15*, *17*) showed that their spin density distributions are very similar, and the largest spin density is at carbon 3 ($\rho^{\pi} \approx 0.5$) where the side chain is attached (see Figure 1). This gives rise to large almost isotropic *hf*-couplings (A_{iso}) of the side chain CH_2 β-protons which dominate the hyperfine pattern of the spectra and which depend both on the neighboring carbon spin density ρ^{π}_C and on the side chain orientation:

$$A_{iso}(H_\beta) = \rho^{\pi}_C(B' + B'' \cos^2 \theta) \qquad (2)$$

$B'$and B'' are empirical constants ($B' = 0$, $B'' = 5$ mT) and θ is the dihedral angle between the adjacent π-carbon (α-carbon) p_z axis and the projected $C_\beta H_\beta$ bond (*17*, *29*, *37*; see Figure 4B). Using eq 2 and assuming approximate tetrahedral geometry, dihedral angles, $\theta_{1,2}$, for β_1, β_2 of 13° and 133° for W111* (*17*) and −90° and 30° for W177* (*15*) were obtained from the ratio of the respective β-proton hyperfine couplings, (see Figure 4B). Thereby the different side chain orientations were determined for both tryptophan radicals, which allowed an assignment to position W111* in the case of R2 from *E. coli* (*17*) and to W177* in the case of R2-Y122W from mouse (*15*) based on comparison with the X-ray structural data (*2*, *3*). Similar large differences of the β-proton hyperfine couplings and related different orientations of the side chain have also been reported for tyrosine radicals in RNR of other organisms (*20*, *38*) and for tyrosine Y_D* in plant photosystem II (*39*).

This work demonstrates that precise *g*-tensor values obtained from high-field EPR are particular useful for identification and characterization of radicals that are immobilized in proteins. Accurate *g*-tensor values including relative orientations of *g*- and *hf*-tensor axes were determined for the first time for protein-associated tryptophan neutral free radicals, which occur in different mutants of RNR. It was shown that tryptophan radicals can be easily distinguished from tyrosine radicals based on their *g*-tensors, which are not affected by different geometries such as, e.g., side chain orientations. The data obtained here for the electronic structure of tryptophan neutral free radicals are important for identification and understanding of catalytically active tryptophan radicals in other enzymes, like, e.g., DNA photolyase, where a coupled tryptophan/flavin radical pair was proposed (*33*), and cytochrome *c* peroxidase (*18*), where a coupled tryptophan/iron-porphyrin system is observed.

ACKNOWLEDGMENT

We thank Profs. B.-M. Sjöberg (Stockholm) and L. Thelander (Umea) for the *E. coli* stems expressing R2 mutants Y122F and Y177W.

REFERENCES

1. Uhlin, U., and Eklund, H. (1994) *Nature 345*, 553.
2. Nordlund, P., and Eklund, H. (1993) *J. Mol. Biol. 232*, 123.
3. Kauppi, B., Nielsen, B. B., Ramaswamy, S., Kjøller-Larsen, I., Thelander, M., Thelander, L., and Eklund, H. (1996) *J. Mol. Biol. 262*, 706.
4. Sjöberg, B.-M. (1997) *Struct. Bonding 88*, 139.
5. (a) Stubbe, J., and Riggs-Gelasco, P. (1998) *Trends Biochem. Sci. 23*, 438. (b) Stubbe, J., and van der Donk, W. A. (1998) *Chem. Rev. 98*, 705−762.
6. Siegbahn, P. E. M. (1998) *J. Am. Chem. Soc. 120*, 8417.
7. Mao, S. S., Holler, T. P., Bollinger, J. M., Johnston, M. I., and Stubbe, J. (1992) *Biochemistry 31*, 9733.
8. Sjöberg, B. M. (1994) *Structure 2*, 793.
9. Siegbahn, P. E. M., Eriksson, L., Himo, F., and Pavlov, M. (1998) *J. Phys. Chem. B 102*, 10622.
10. Atkin, C. L., Thelander, L., Reichard, P., and Lang, G. (1973) *J. Biol. Chem. 248*, 7464.
11. Sahlin, M., Lassmann, G., Pötsch, S., Slaby, A., Sjöberg, B.-M., and Gräslund, A. (1994) *J. Biol. Chem. 269*, 11699.
12. Sturgeon, B. E., Burdi, D., Chen, S., Huynh, B.-H., Edmondson, D. E., Stubbe, J., and Hoffman, B. M. (1996) *J. Am. Chem. Soc. 118*, 7551.
13. Ravi, N., Bollinger, J. M., Huynh, B. H., Edmondson, D. E., and Stubbe, J. (1994) *J. Am. Chem. Soc. 116*, 8007.
14. Kolberg, M., Bleifuss, G., Pötsch, S., Gräslund, A., Lubitz, W., Lassmann, G., and Lendzian, F. (2000) *J. Am. Chem. Soc. 122*, 9856−9857.
15. Pötsch, S., Lendzian, F., Ingemarson, R., Hörnberg, A., Thelander, L., Lubitz, W., Lassmann, G., and Gräslund, A. (1999) *J. Biol. Chem. 274*, 17696.
16. Sahlin, M., Lassmann, G., Pötsch, S., Sjöberg, B.-M., and Gräslund, A. (1995) *J. Biol. Chem. 270*, 12361.
17. Lendzian, F., Sahlin, M., MacMillan, F., Bittl, R., Fiege, R., Pötsch, S., Sjöberg, B.-M., Gräslund, A., Lubitz, W., and Lassmann, G. (1996) *J. Am. Chem. Soc. 118*, 8111.
18. Huyett, J. E., Doan, P. E., Gurbiel, R., Houseman, A. L. P., Sivaraja, M., Goodin, D. B., and Hoffman, B. M. (1995) *J. Am. Chem. Soc. 117*, 9033.
19. Andersson, K. K., and Gräslund, A. (1995) in *Advances in Inorganic Chemistry*, p 359, Academic Press, Orlando, FL.
20. van Dam, P. J., Willems, J.-P., Schmidt, P. P., Pötsch, S., Barra, A.-L., Hagen, W. R., Hoffman, B. M., Andersson, K. K., and Gräslund, A. (1998) *J. Am. Chem. Soc. 120*, 5080.
21. Stesmans, A., and VanGorp, G. (1989) *Rev. Sci. Instrum. 60*, 2949.
22. Rieger, P. H. (1982) *J. Magn. Reson. 50*, 485−489.
23. Mombourquette, H. J., and Weil, J. E. (1992) *J. Magn. Reson. 99*, 37−44.
24. (a) ADF Release 2000.02, Scientific Computing and Modelling NV, Theoretical Chemistry, Vrije Universiteit Amsterdam, The Netherlands; (b) Baerends, E. J., Ellis, D. E., and Ros, P. (1973) *Chem. Phys. 2*, 41; (c) Versluis, L., and Ziegler, T. (1988) *J. Chem. Phys. 88*, 322; (c) te Velde, G., and Baerends, E. J. (1992) *J. Comput. Phys. 99*, 84; (d) Fonseca Guerra, C., Snijders, J. G., te Velde, G., and Baerends, E. J. (1998) *Theor. Chem. Acc. 99*, 391.
25. Becke, A. D. (1988) *Phys. Rev. A 38*, 3098.
26. Perdew, J. P. (1986) *Phys. Rev. B 33*, 8822.
27. Burghaus, O., Plato, M., Rohrer, M., Möbius, K., MacMillan, F., and Lubitz, W. (1993) *J. Phys. Chem. 97*, 7639.
28. Stone, A. J. (1963) *Proc. R. Soc. London, Ser. A A271*, 424.
29. Carrington, A., and McLachlan, A. D. (1969) *Introduction to Magnetic Resonance*, Harper & Row, New York.

30. Un, S., Gerez, C., Elleingand, E., and Fontecave, M. (2001) *J. Am. Chem. Soc. 123*, 3048−3054.
31. Engström, M., Himo, F., Gräslund, A., Minaev, B., Vahtras, O., and Agren, H. (2000) *J. Phys. Chem. A 104*, 5149.
32. Himo, F., Gräslund, A., and Eriksson, L. A. (1997) *Biophys. J. 72*, 1556−1567.
33. Gindt, Y. M., Vollenbroeck, E., Westphal, K., Sackett, H., Sancar, A., and Babcock, G. (1999) *Biochemistry 38*, 3857.
34. Gerfen, G. S., Bellew, B. F., Un, S., Bollinger, J. M., Jr., Stubbe, J., Griffin, R. G., and Singel, D. J. (1993) *J. Am. Chem. Soc. 115*, 6420−6421.
35. Nimz, O., Lendzian, F., Boullais, C., and Lubitz, W. (1998) *Appl. Magn. Reson. 14*, 255.
36. Chasteen, N. D., and Francavilla, J. (1976) *J. Phys. Chem. 80*, 867.
37. Stone, E. W., and Maki, A. H. (1962) *J. Chem. Phys. 37*, 1326.
38. Allard, P., Barra, A. L., Andersson, K. K., Schmidt, P. P., Atta, M., and Gräslund, A. (1996) *J. Am. Chem. Soc. 118*, 895.
39. Un, S., Tang, X.-S., and Diner, B. (1996) *Biochemistry 35*, 679.
40. Babcock, G. T., Espe, M., Hoganson, C., Lydakis-Simantiris, N., McCracken, J., Shi, W., Styring, S., Tommos, C., and Warncke, K. (1997) *Acta Chem. Scand. 51*, 533−540.
41. Hoganson, C. W., Sahlin, M., Sjöberg, B.-M., and Babcock, G. T. (1996) *J. Am. Chem. Soc. 118*, 4672.
42. Bender, C. J., Sahlin, M., Babcock, G. T., Barry, B. A., Chandrashekar, T. K., Salowe, S. P., Stubbe, J., Lindström, B., Peterson, L., Ehrenberg, A., and Sjöberg, B.-M. (1989) *J. Am. Chem. Soc. 111*, 8076.

BI010707D